Electronic Supplementary Material (ESI) for Materials Advances.

Supplementary Information

Self-cleaning formulation of mixed metal oxide-silver micro-nano structures with spiky corona as antimicrobial coatings for fabrics and surfaces

Ramya Prabhu B.[1],[†] Bhamy Maithry Shenoy[2],[†] Manish Verma[1], Soumyashant Nayak[3], Gopalkrishna Hegde[2], Neena S. John[1]*

[1]Centre for Nano and Soft Matter Sciences, Shivanapura, Bengaluru 562162, India

[2]Indian Institute of Science, Bengaluru 560012

[3]Theoretical Statistics and Mathematics Unit, Indian Statistical Institute, Bengaluru 560059, India

[†]Equal Contribution

Email: jsneena@cens.res.in

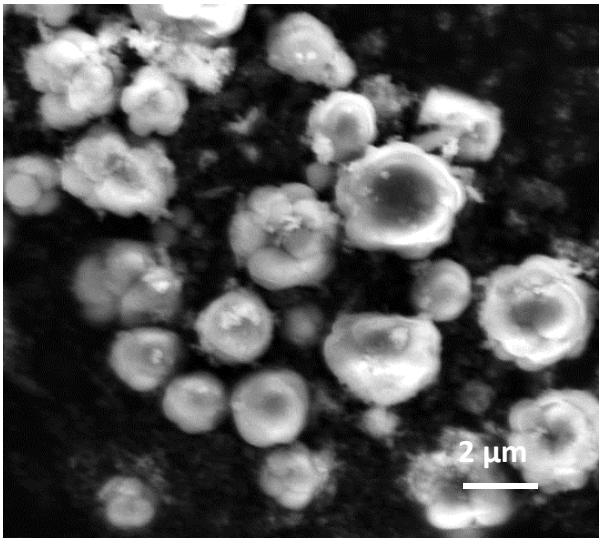

Figure S1. FESEM images of spherical MMO-Ag.

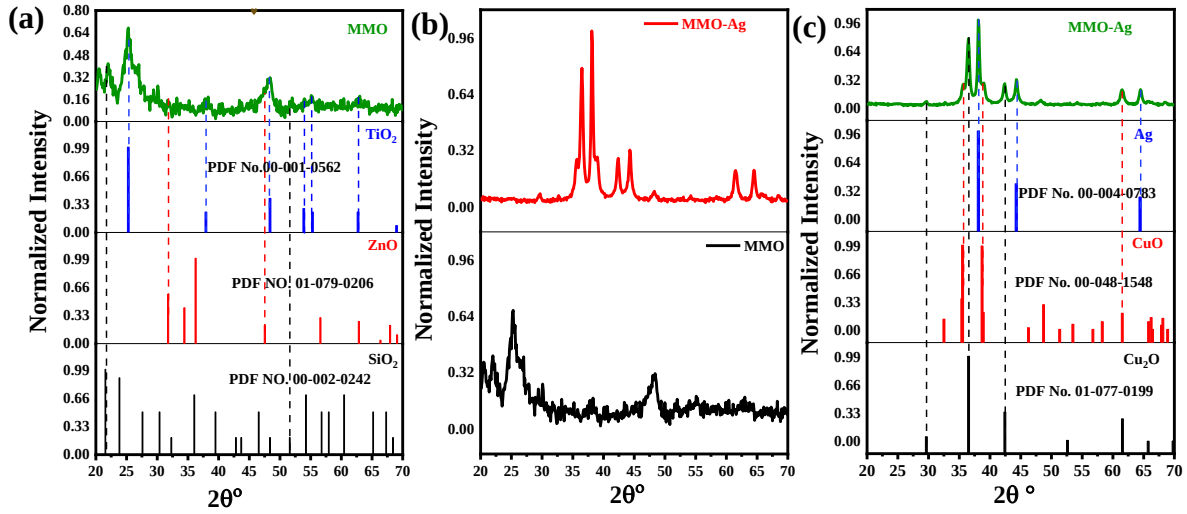

Figure S2. X-ray diffractograms (a) spiky MMO (b) comparison of MMO-Ag and MMO (c) MMO-Ag

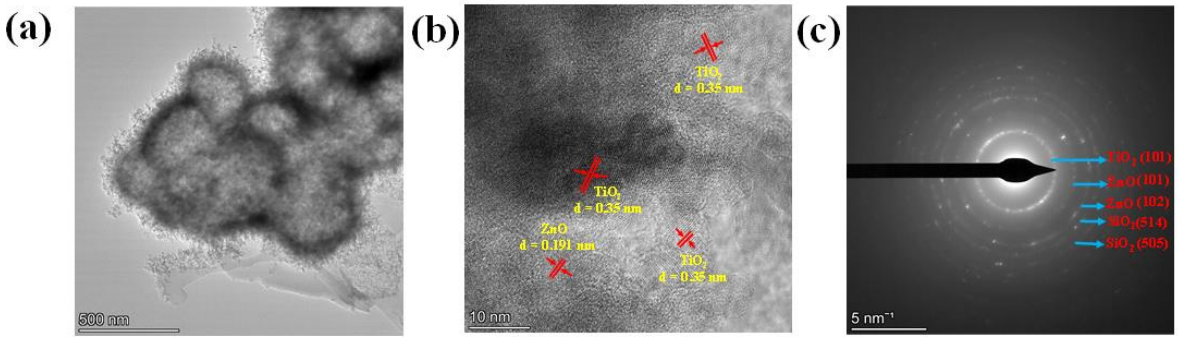

Figure S3. Additional TEM images (a) spiky MMO (b) HRTEM analysis of MMO (c) SAED analysis of MMO

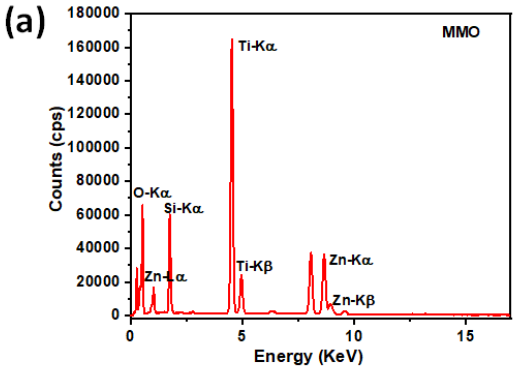

(b)

Element	At (%)
O (K)	32.05
Ti (K)	41
Si (K)	13.44
Zn (K)	13.5

Figure S4. EDS of MMO obtained from TEM

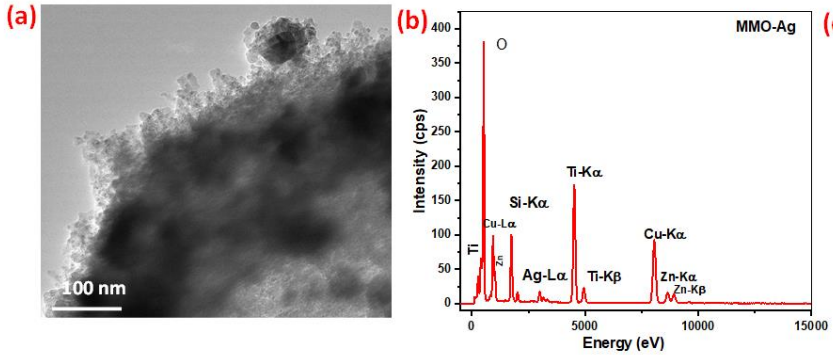

(c)

Element	At (%)
O (K)	32.05
Ti (K)	41
Si (K)	13.44
Cu (K)	12.6
Zn (K)	2.9
Ag (L)	1.1

Figure S5. a) Magnified TEM image of MMO-Ag (b,c) EDS of MMO-Ag obtained from TEM

XPS Study

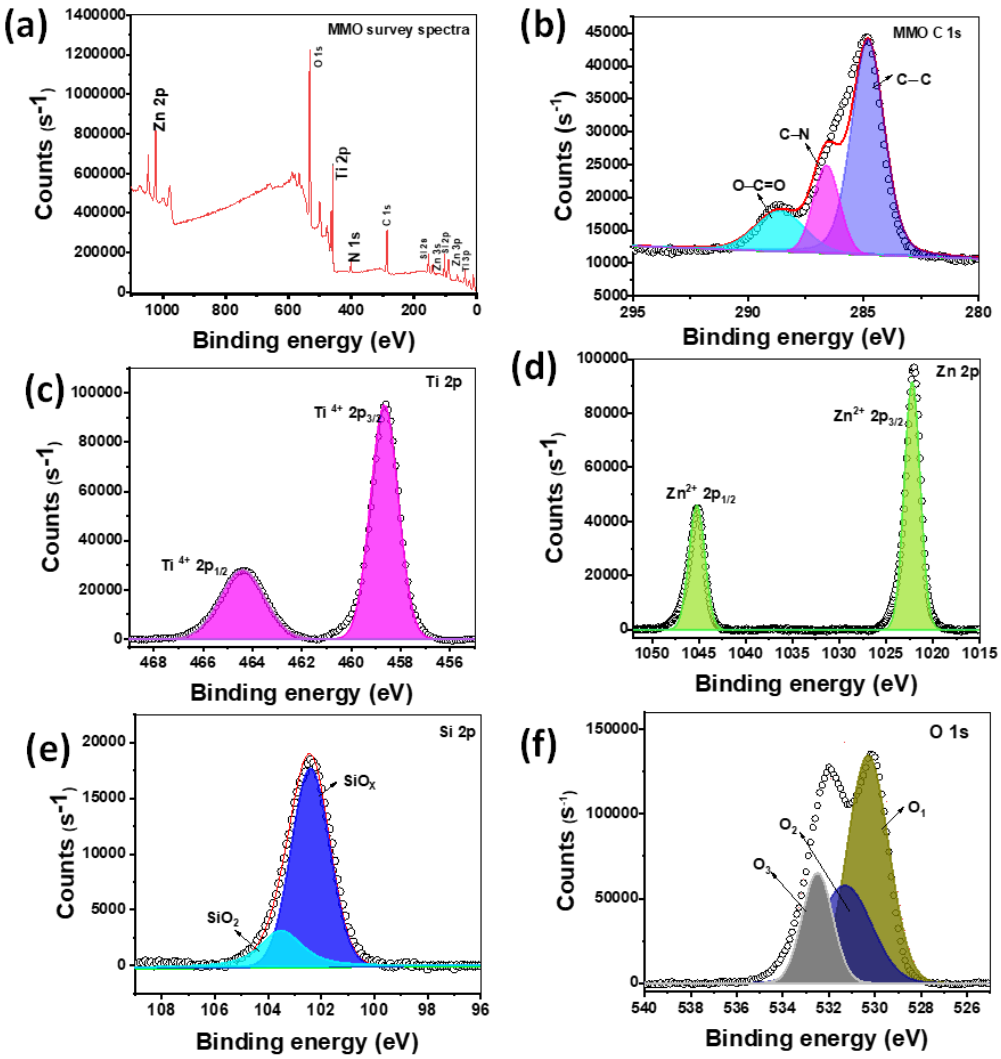

Figure S6. XPS spectra of MMO (a) XPS survey spectra of MMO. High-resolution XPS of (b) C 1s (c) Ti 2p (d) Zn 2p (e) Si 2p (f) O 1s.

The surface oxidation states of various elements in the MMO have been studied using XPS, as shown in Figure S6. The XPS survey scan (Figure S6(a)) reveals the presence of signatures of Ti (2p, 3p), Si (2s,2p), Zn (2p,3s, 3p), N (1s), C (1s) and O (1s). The deconvoluted high-resolution C1s spectra are presented in Figure S6(b), in which the peaks observed at 284.8 eV correspond to sp^2 and sp^3carbon. The peaks around 286 eV and 288.4 eV can be attributed to C-N (of HMTA) and O-C=O (of oxalate), respectively [*Md. Nizam Uddin et al., Thin Solid Films, **2013** ,548, 27-33; B. Kommula et al., Part. Part. Syst. Charact. **2023,** 2300118*].The Ti 2p peaks can be deconvoluted and assigned to $2p_{3/2}$ (458.6 eV) and $2p_{1/2}$ (464.4 eV) of Ti^{4+} oxidation states arising from TiO_2 (Fig. S6 (c)) [*S.C. Ray et al., J. Phys. Chem. C **2022**, 126 (20), 8947*]. The Zn 2p spectra reveal the presence of Zn^{2+} $2p_{3/2}$ and Zn^{2+} $2p_{1/2}$ peaks centered at 1022.1 eV and 1045.1 eV, respectively as shown in Fig.S6(d) corresponding to ZnO in MMO [D. L.T. Nguyen et al., *ACS Sustain. Chem. Eng. **2017**, 5 (12), 11377–11386*]. The deconvolution of Si 2p spectra reveals the presence of low valent Si in nonstoichiometric SiO_x (102.4 eV) and Si^{4+} in SiO_2 (103.5 eV) (Figure S6(e) [*R. Alfonsetti et al., Appl. Surf. Sci. 1993, 70–71, 222; Surf. Interface Anal. 1994, 22 (1–12), 89,L. Sun et al., ACS Appl. Mater. Interfaces **2017**, 9 (46), 40386*]. The O 1s spectra is deconvoluted into three peaks at 530.2 eV (O_1) corresponding to the oxide ion (O^{2-}) forming the metal-oxygen bond, 531.3 eV (O_2) corresponding to oxygen-deficient species and 532.5 eV (O_3), attributed to the surface hydroxyl groups (Figure S6(f)) [*R. Prabhu B., et al., Nanotechnology **2023**, 34 (21), 215701*]. The relative percentage intensity of O_1, O_2, O_3 species is 52.25%, 28.85 %, and 18.89 %. From the XPS analysis, it is evident that the synthesized material contains an adequate amount of defective oxygen.

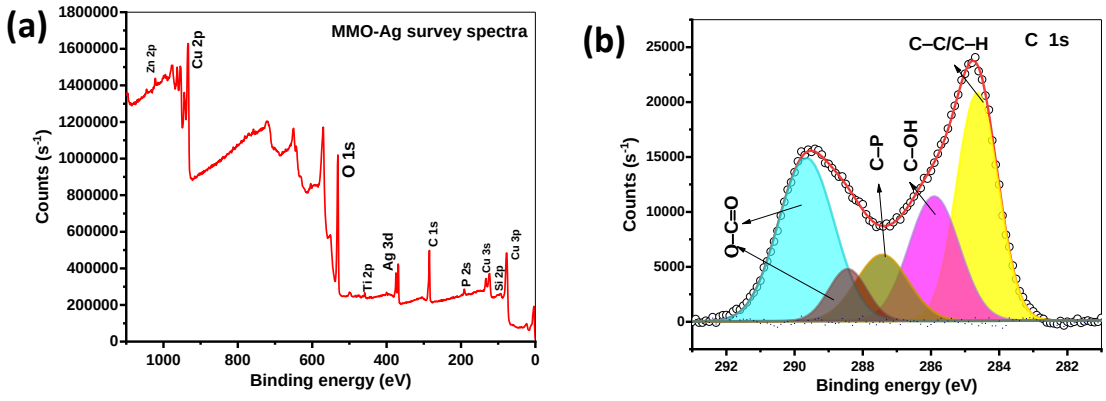

Figure S7. (a) XPS survey spectra of MMO-Ag (b) High-resolution XPS of C1s

The XPS survey scan of MMO-Ag (Figure S7(a)) reveals the presence of major transitions due to Ti (2p, 3p), Si (2s,2p), Zn (2p,3s, 3p), N (1s), C (1s) and O (1s) similar to MMO. In addition, signals from P (2s), Cu (2p,3s,3p), Ag(3d) are also detected in MMO-Ag as expected due to the presence of CuO, Ag and THPC.

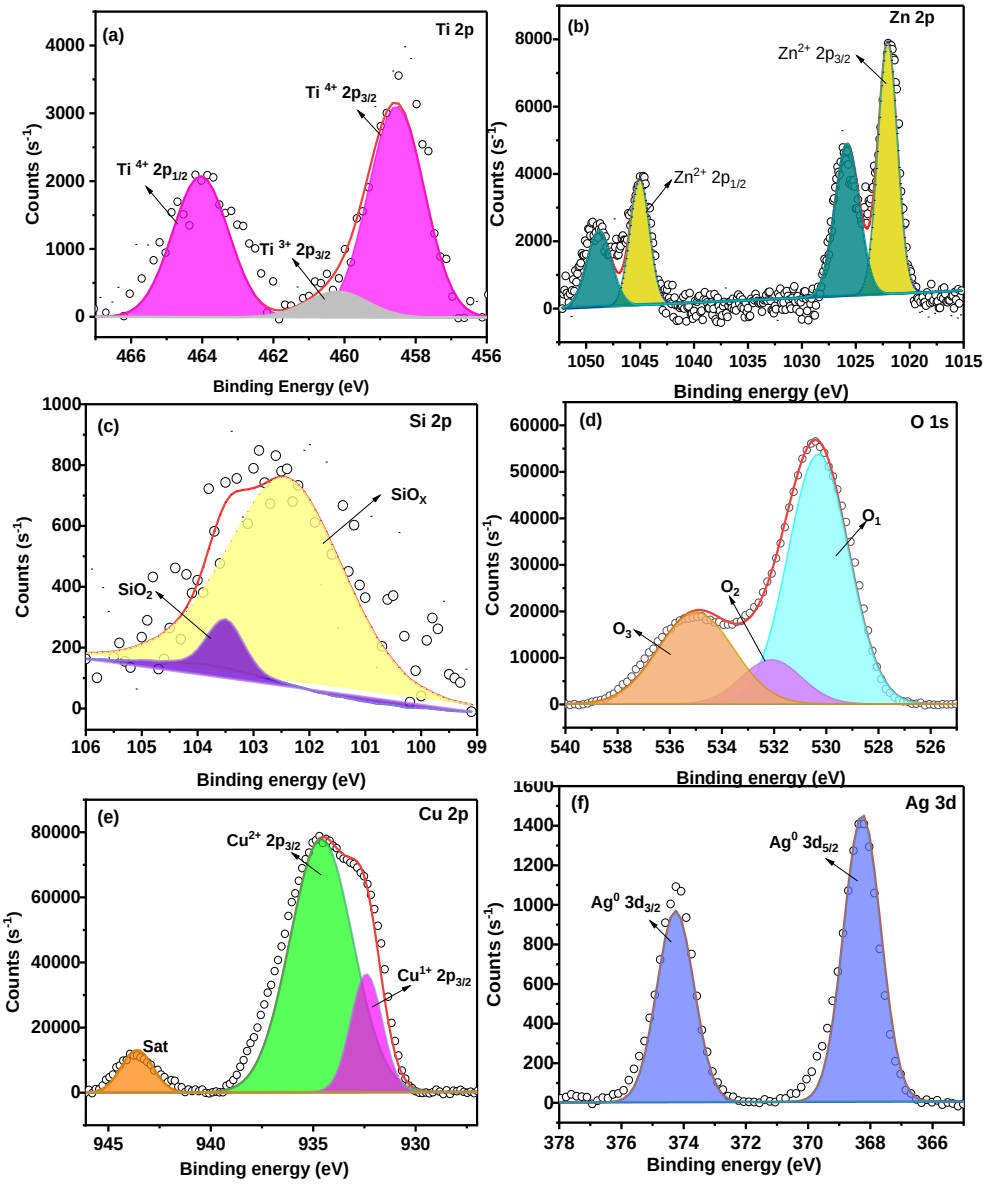

Figure S8. XPS spectra of MMO-Ag (after deposition of CuO and Ag on MMO). High-resolution XPS of (a) Ti 2p, (b) Zn 2p, (c) Si 2p, (d) O 1s, (e) Cu 2p, (f) Ag 3d.

The deconvoluted high-resolution C1s spectra (Fig. S7(b)) exhibits peaks at 284.6 eV that correspond to sp^2/sp^3 C-C and C-H. The peaks around 285.9 eV, 287.4 eV, 288.4 eV and 289.6 eV can be attributed to C-N (HMTA)/C-OH (THPC), C-P/C-O-C (oxalate, THPC), and C=O/O-C=O groups (hydrolysed and oxidised THPC products), respectively [*T.R.*

Gengenbach et al., J. Vac. Sci. Technol. A 2021, 39, 013204, Z. Bian et al., IOP Conf. Ser.: Mater. Sci. Eng. 2017, 242, 012005].

The Ti 2p peaks of MMO-Ag can be deconvoluted and assigned to $2p_{3/2}$ (458.5 eV) and $2p_{1/2}$ (463.9 eV) corresponding to Ti^{4+} oxidation state of TiO_2 (Fig. S8(a)). In addition to these peaks, a weak peak is observed at 460.1 eV that can be assigned to Ti^{3+}due to titanium suboxide [*B. Bharti et al., Sci. Rep. 2016, 6 (1), 32355*]. The alkaline treatment followed by chemical reduction would have resulted in the suboxide formation. In the case of Zn 2p spectra, in addition to the presence of Zn^{2+} $2p_{3/2}$ and $2p_{1/2}$ peaks at 1022.0 eV and 1045.0 eV, respectively as shown in Fig. S8(b), peaks at a higher binding energy,1025.8 eV and 1048.8 eV are also observed. This can be associated with the coordination of Zn with the surfactants such as hydrolysed THPC [*L.G. Mar et al., Thin Solid Films, 1993, 223, 341*]. Similarly, as in the case of MMO the deconvolution of Si 2p spectra shows the presence of majorly low valent Si from nonstoichiometric SiOx (102.4 eV) and SiO_2 (103.5 eV), respectively (Fig. S8(c)). The O 1s peak of MMO-Ag nanoformulations can be deconvoluted into three peaks, as depicted in Figure S8(d). The O_1 (lattice oxygen) at a lower binding energy value of 530.3 eV, O_2 around 532.0 eV due to the hydrated species a broader peak at 534.9 eV (O_3) is due to the H_2O molecules. Figure S8 (e) shows the deconvoluted spectra of Cu 2p. The Cu $2p_{3/2}$ component can be deconvoluted into peaks contributed by Cu^{1+} and Cu^{2+} states, located at 932.3 and 934.5 eV. This clearly shows the presence of Cu_2O and CuO and agrees with the XRD results. [*D. A. Svintsitskiy, J. Phys. Chem. C 2013, 117, 28, 14588*] The satellite peak with a binding energy of 943.6 eV is also observed in the spectra. The HRXPS of Ag 3d indicates the presence of elemental silver (Ag^0) at 368.2 eV ($3d_{5/2}$) and 374.2 eV ($3d_{3/2}$), respectively (Figure S8(f)) [*W.W. Bryan et al., RSC Adv., 2016, 6, 68150*].

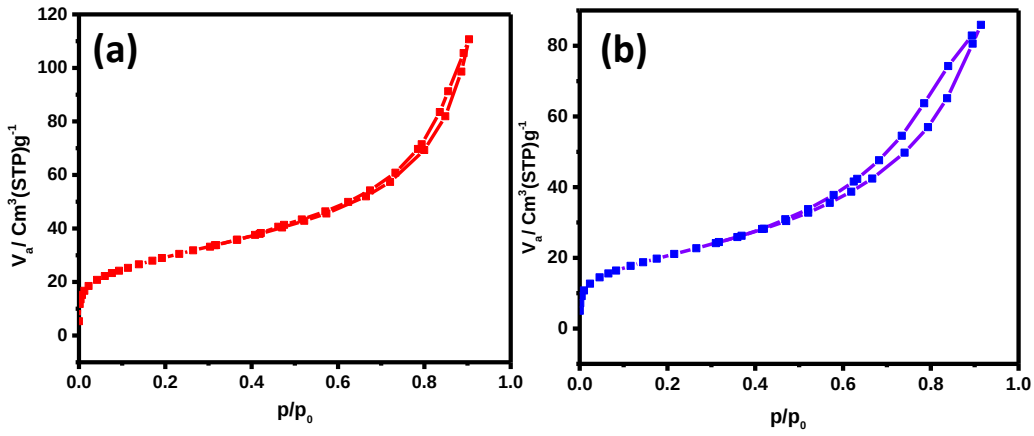

Figure S9. BET isotherm and BJH plot, respectively of (a, b) MMO (c, d) MMO-Ag.

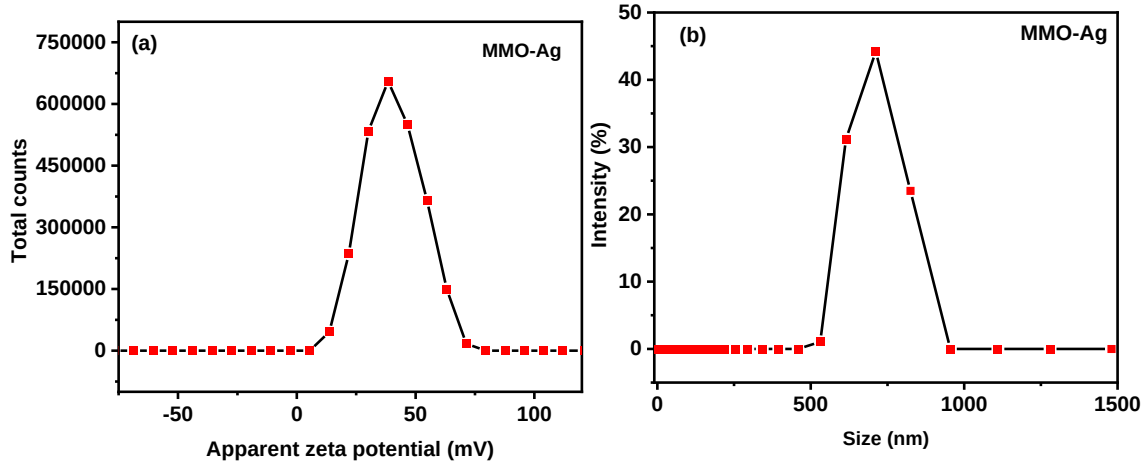

Figure S10. (a) Zeta potential plot (b) Average particle size distribution of 1 mg/mL concentration of MMO-Ag in ethanol by DLS.

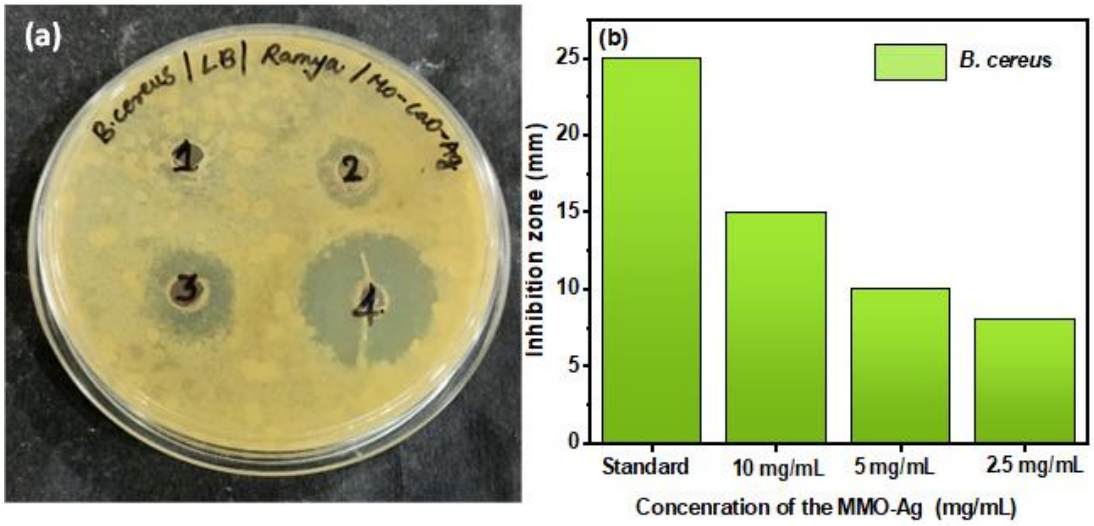

Figure S11. Photographs of ZI (a) MMO-Ag against *B. cereus. (*b) Bar diagrams showing ZI for various concentrations of MMO-Ag along with that of the standard antibiotic Ciprofloxacin.

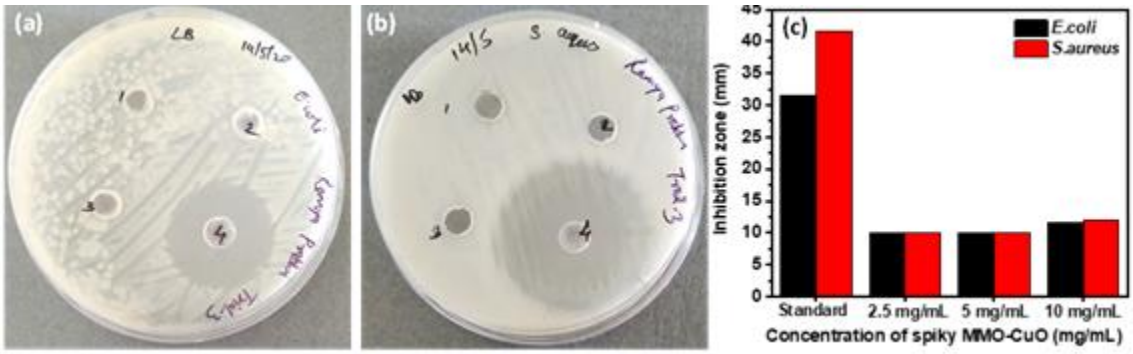

Figure S12. Photographs of ZI obtained for various concentrations of spiky MMO-CuO (without Ag) (a) against *E. coli* (b) against *S. aureus* (c) Bar diagrams showing ZI.

The numbers 1, 2, and 3 in the photographs correspond to the loading of 2.5, 5, and 10 mg/mL of the spiky MMO-CuO on the test bacteria, respectively and number 4 corresponds to the standard antibiotic ciprofloxacin. The corresponding inhibition zone values are shown in the bar graph, Figure S12(c). It is observed that spiky MMO-CuO has slightly lesser antimicrobial properties (lesser ZI) compared to the spiky MMO-Ag , but is still active.

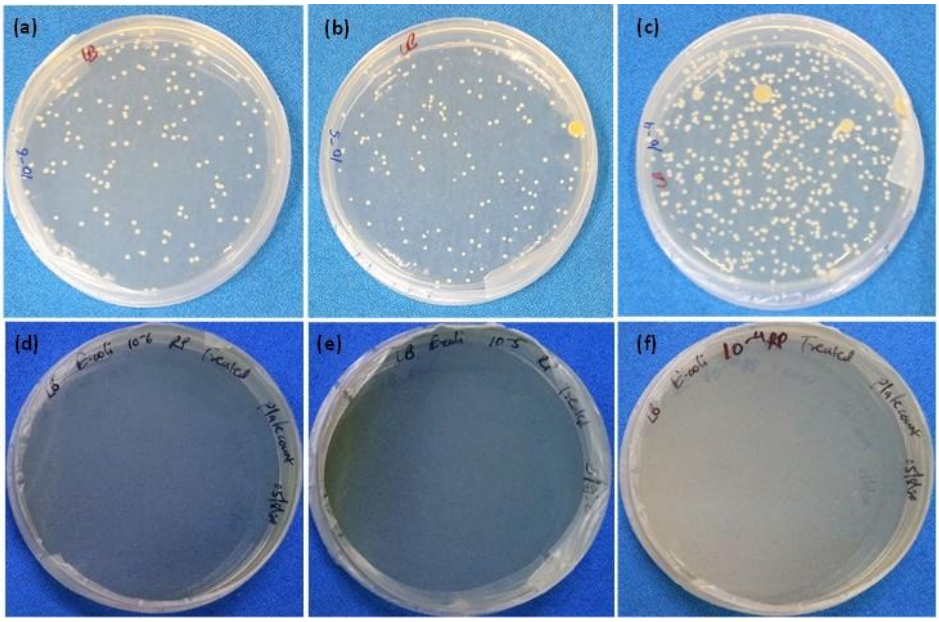

Figure S13. Photographs of agar plates incubated with (a-c) *E. coli* of 8×10^{-6}, 8×10^{-5} and 8 $x10^{-4}$ CFU/mL (d-f) treated with 10 mg/mL MMO-Ag.

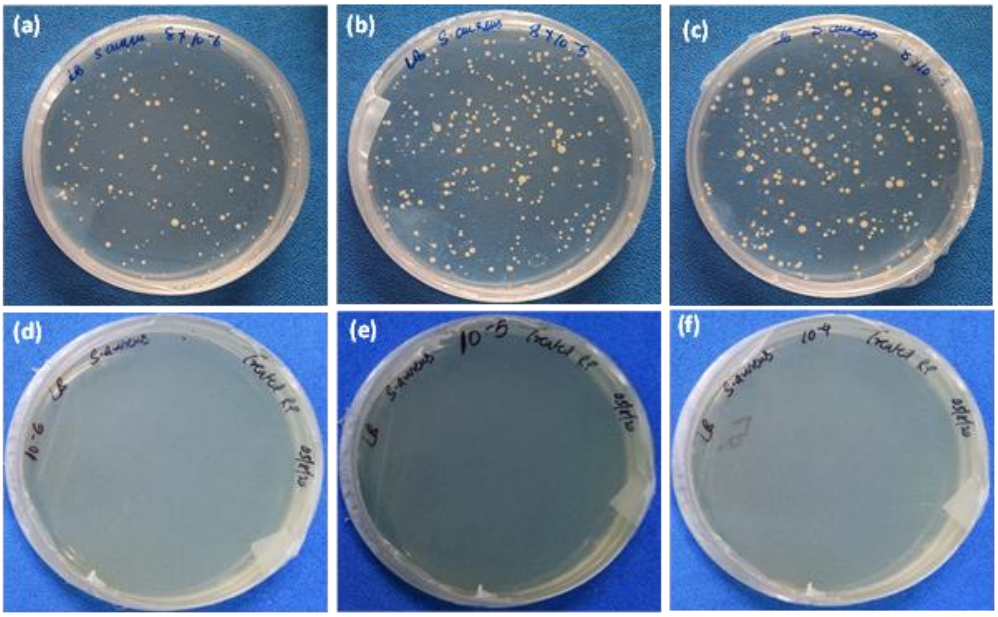

Figure S14. Photographs of agar plates incubated with (a-c) *S. aureus* of 8×10^{-6}, 8×10^{-5} and 8 $x10^{-4}$ CFU/mL (d-f) treated with 10 mg/mL MMO-Ag.

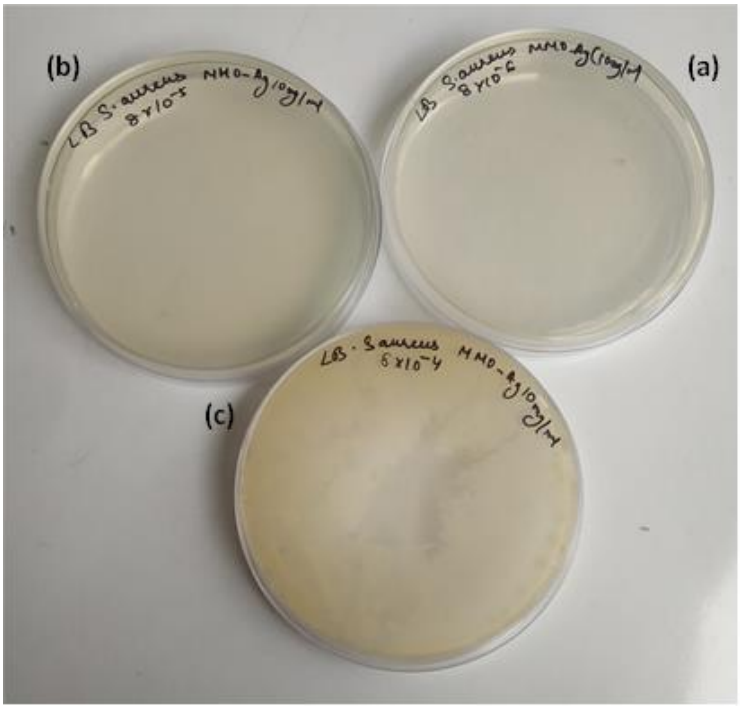

Figure S15. Photographs of agar plates incubated with (a-c) S. aureus of 8×10^{-6}, 8×10^{-5}, and 8 $x10^{-4}$ CFU/mL treated with 10 mg/mL spherical MMO-Ag.

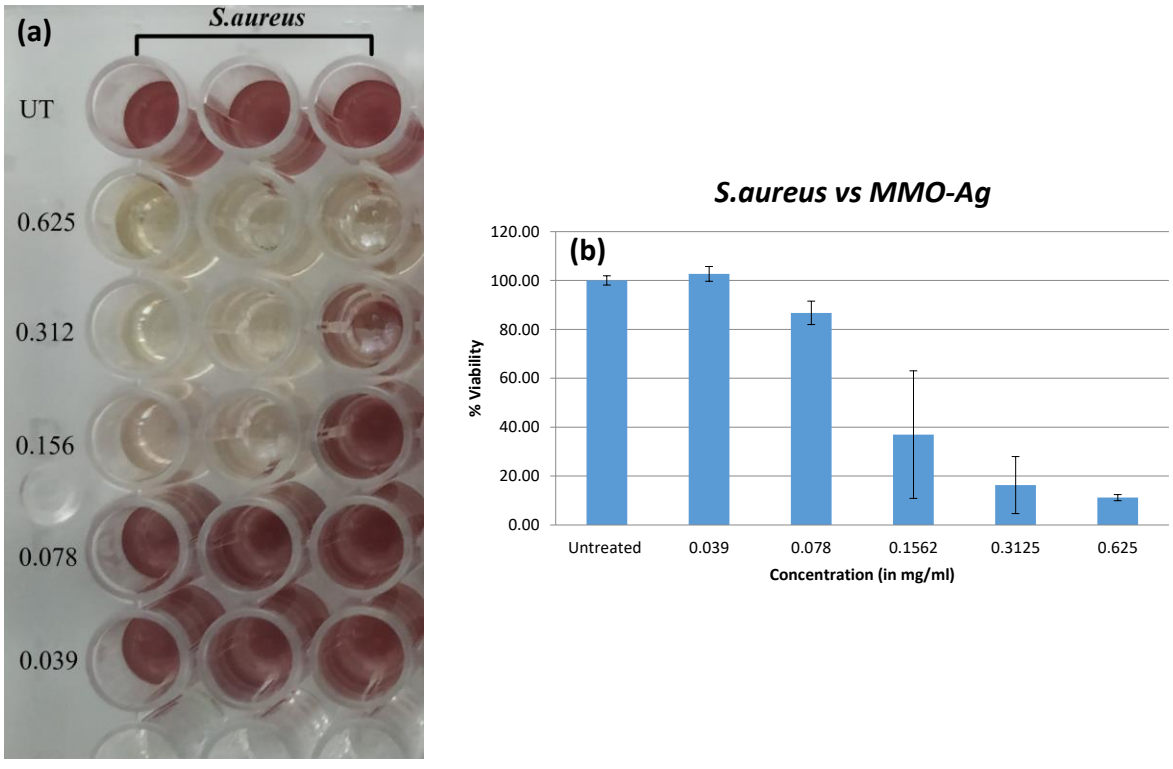

Figure S16. Photographs of 96 wells microtitre plate with *S. aureus* bacterial solution treated with various concentrations of (a) MMO-Ag (b) Graph showing percentage viability of *S. aureus* vs. MMO-Ag.

We can observe the untreated *S. aureus* bacteria is well-grown in the media and the red turbidity is observed. That is because the ρ-iodonitrotetrazolium violet dye which is treated with the microorganism has reduced to form a purple formazan dye. The reduction of the tetrazolium salt is due to the activity of the mitochondria enzyme in the active cells [*J.N. Eloff et al., Planta Med. 1998, 64, 711*]. The intensity of the formazan compound can be measured using absorbance where the intensity of the compound is directly proportional to the number of metabolically active cells. From these microplate's absorbance is recorded at the 600 nm wavelength, and the cell viability is calculated.

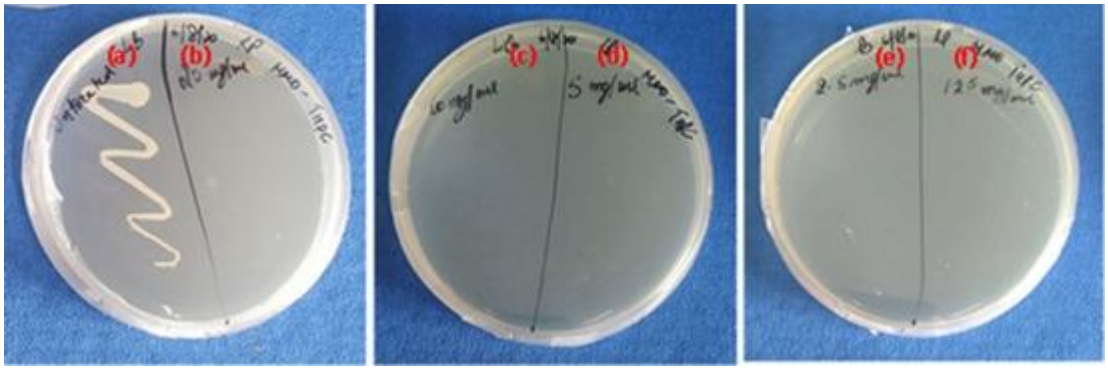

Figure S17. Photographs of agar plate with *S. aureus* bacterial solution (a) untreated agar plate (b) treated with 20 mg/mL (c) 10 mg/mL (d) 5 mg/mL (e) 2.5 mg/mL (f) 1.25 mg/mL concentration of the MMO-Ag.

Table S1. Comparison of antibacterial activity with literature

Nanomaterial	**Size & Shape**	**Microbe**	**Mode of action**	**Efficacy against microbes**	**Ref**
MMO-Ag	**~1.2 µm spiky**	**Gram-positive and gram-negative bacteria and virus**	**ROS generation, mechano-bactericidal effect, Electrostatic interaction**	**MIC_{50} 107µg/mL -*S. aureus***	**This work**
CuO-NiO	8–10 nm nanoparticles	Gram-positive and Gram-negative bacteria	electrostatic force of attraction	MIC 3.0 mg/mL -*S. aureus* 4.9 mg/mL -*E. Coli*	Mater. Res. Exp., 2019, 6(5), 055004.
ZnO nanoparticles in ionic liquid	64 nm nanoparticles	Gram-positive bacteria *S. epidermidis*, Skin specific bacteria	toxic Zn2+ ions are produced, which in turn help in the production of intracellular ROS	IC_{50} 70 µg/mL and IC_{90} 105 for *S. epidermidis*	ACS Appl. Mater. Interfaces 2018, 10, 18, 15401.
CoV_2O_6	10-200 nm Nanorods	Gram-positive and Gram-negative bacteria	Electrostatic interaction of the Co metals and the membrane	IC_{50} 0.43 mg/mL- *E. Coli* 0.51 mg/mL *Kleb. p* 0.53 mg/mL-*MRSA*	Ceramics Int., 2018, 44(7), 7716.

			Oxidative stress in cells and DNA damage	0.62 mg/mL-S. aureus	
Cellulose/Yttrium oxide	Nanodisc on nanotube	Gram-positive and Gram-negative bacteria	photocatalytic disinfection Generation of reactive species	~100% efficacy 30 mg/L- *E. Coli* 60 mg/L-*S. aureus*	Mater. Lett., 2017, 192, 64.
Silver/Lithium /Vanadium oxide	Nanotube Dia 40-50 nm	Gram-positive and Gram-negative bacteria	direct action of the nanocomposites on the cell surfaces by generation of ROS	MIC_{50} 40 µg/mL-*B. subtilis* 80 µg/mL- *E. Coli*	Appl. Microbiol. Biotechnol., 2013, 97(18), 283.
mesoporous silica supported SBA/CuO SBA/ZnO CuZnO	Spherical	Gram-positive and Gram-negative bacteria	Release of dissociated metal ions and the release of reactive oxygen species	12.5 mg/mL 50 mg/mL 0.558 mg/mL-*E. coli* 3.125 mg/mL 12.5 mg/mL 0.139 mg/mL-*S. aureus*	RSC Adv., 2020,10, 2767.
RGO-NiO, RGO-AgO, RGO-ZnO	rGO sheets metal oxide spherical nanoparticles	Gram-positive and Gram-negative bacteria	the release of reactive oxygen species	250 µg/mL 250 µg/mL 125 µg/mL-*E. coli* 125 µg/mL 25 µg/mL 250 µg/mL-*S. aureus*	RSC Adv., 2021,11, 25961.
CuO ZnO	Nanorods Average length 100 nm Spherical 10 nm to 35 nm	Gram-positive and Gram-negative bacteria	the release of reactive oxygen species	1 mg/mL-*E. coli* 0.25 mg/mL *S. aureus* 0.1 mg/mL- *S. aureus* No inhibition-*E. coli*	Results in Materials, 2020, 7, 100099
Ag-Sn/SnO_2 Ag Sn/SnO_2	Particle size 1–18 nm in size. rod type, chain like and interlinked with each other	Gram-negative bacteria	Ag/Ag+ enters inside the cell through phagocytosis/endocytosis, then it can damage the DNA and the release of reactive oxygen species	0.015 µg/mL 0.03 µg/mL 0.625 µg/mL - *A. baumanii*	RSC Adv., 2022, 12, 1105
α-Fe_2O_3/Co_3O_4 (0.1(M) Fe_2O_3+ 0.1(M) Co_3O_4)	Mix of rod shaped and roughly hexagonal shaped nanoparticles	Gram-positive and Gram-negative bacteria	Fenton reaction cobalt oxide nanoparticles trigger the production of reactive oxygen species	90 mg/dL-*B. subtilis* 75 mg/dL-*S. aureus* 60 mg/dL-*S. typhi* 45 mg/dL-*E.coli*	Appl. Nanosci. , 2018, 8, 137.
WO_3-GO	WO_3 nanospheres on the graphene	Gram-positive and Gram-	photocatalytic antibacterial effect	2.5-5 mg/mL	J. Phys. Chem. Solids,

	sheet	negative bacteria			2018, 116,137.
Li-doped MgO	thin sheets	Gram-positive and Gram-negative bacteria	Generation of holes and free electrons by defect rich MgO mechanical damage by sheet morphology	600 µg/mL-against *E. coli* and *S. aureus*	Powder Tech., 2020, 371, 130.
ZnO @ rattle-type silica nanoparticles (ZnO@SN)	Silica has inner hollow cavity of 150 nm size and a rough shell studded with many 4-6 nm ZnO nanoparticles	Gram-negative bacteria	ROS from ZnO particles	6.25 µg/mL methicillin-resistant Staphylococcus aureus	Sci. Bull. 2017, 62, 1207.
Ag/CuO 5%	Ag nanoparticles CuO porous open channel	Gram-positive and Gram-negative bacteria	ROS	30 µg/mL- *E. coli* 30 µg/mL-*K. pneumoniae* 20 µg/mL-*S. aureus*	Colloids Surf A, 2019, 580, 123732
Ag@MgO	Embedded-layered coreshell structure with 3-10 nm size	Gram-positive and Gram-negative bacteria	Release of Ag^{+} and Mg^{2+} ions as well as the production of reactive oxygen species	15 µg/mL- *E. coli* 20 µg/mL-*S. aureus*	Photodiagnosis and Photodynamic Therapy, 2021, 33, 102153
Nanostructured Ti surface	Nanowire/Nano sheet clusters on surface with 23 nm pyramidal tip	Gram-positive and Gram-negative bacteria	Mechanobactericidal effect	bactericidal efficiency of 98.6 ± 1.23% against *E. coli* and 69.82 ± 2.79% against *S. aureus*	ACS Biomater. Sci. Eng. 2021, 7, 2268
High aspect ratio vertically aligned carbon nanotubes	100-3000 aspect ratio CNTs	Gram-positive and Gram-negative bacteria	Mechanobactericidal effect	bactericidal rates of 99.3% for *P. aeruginosa* and 84.9% for *S. aureus*	ACS Nano 2018, 12, 7, 6657

Table S2. Antibacterial activity of meltblown fabric coated with nanoformulation

Area of the zone of inhibition in (mm^2) Diameter of plate – 90 mm			
Microorganism	**Sample**	**Area of textile sample (mm^2)**	**Area of Zone of inhibition (mm^2)**
E.coli	MMO-Ag	190	273
		95	200
S. aureus	MMO-Ag	176	300
		189	325

Table S3. Antiviral testing against bacteriophage virus

Sample Identification	Test organism MS2 Bacteriophage				Log reduction** of virus at 2h	%e reduction***of virus at 2h	MS2 Bacteriophage		Log reduction of virus at 24 h	%reduction of virus at 24 h
	Average PFU/carrier at 0 hours (B)		Average PFU/carrier at 2 h(A)				Average PFU/carrier at 24 h(A)			
	PFU*	log	PFU	log			PFU	log		
Nonwoven fabric(coated with nanoformulation)	7.1×10^4	4.85	5.60×10^2	2.74	2.11	99.21	4.00×10^3	3.60	1.25	94.36
Lab control(untreated nonwoven fabric)			9.20×10^4	4.96	4.96	0.00	9.60×10^4	4.98	0.00	0.00

*PFU: Plaque Forming Unit = No. of Microorganisms

** Log reduction Log (B/A) Percentage

*** reduction = (B – A/ B) x 100; where B is the number of viable test microorganisms on the control carriers immediately after inoculation and A Number of viable test microorganisms on the test carriers after the contact time.

Cytotoxicity Assay

The cytotoxicity of the MMO-Ag is evaluated by the Cytotoxicity Assay Method. The assay is done in a 96-well plate format in 3 wells for the sample. $1x10e^4$ VeroE6 cells were plated per well and incubated at 37 °C overnight for the monolayer formation. The next day, cells were incubated with the MMO-Ag at 10 mg/mL, 1 mg/mL, and 0.5 mg/mL concentration. The cells without the MMO-Ag were the control. 24 and 48 hours later, cells were stained with Hoechst 33342 and Sytox orange dye. Images were taken at 10X magnification, 16 images per well, which covers 90% of the well area using Image Xpress Micro confocal (Molecular Devices). Hoechst 33342 nucleic acid stain is a popular cell-permeant nuclear counterstain that emits blue fluorescence when bound to dsDNA. It stains all the live and dead cells. Sytox orange dye stains nucleic acids in cells with compromised membranes. This stain is an indicator of cell death. First, the software will count the total number of cells in the Hoechst image. In the Sytox image, it will count, among Hoechst positive cells, how many cells are positive for Sytox. From the below results, we can conclude that MMO-Ag at 1 mg/mL and 0.5 mg/mL is not cytotoxic on VeroE6 cells.

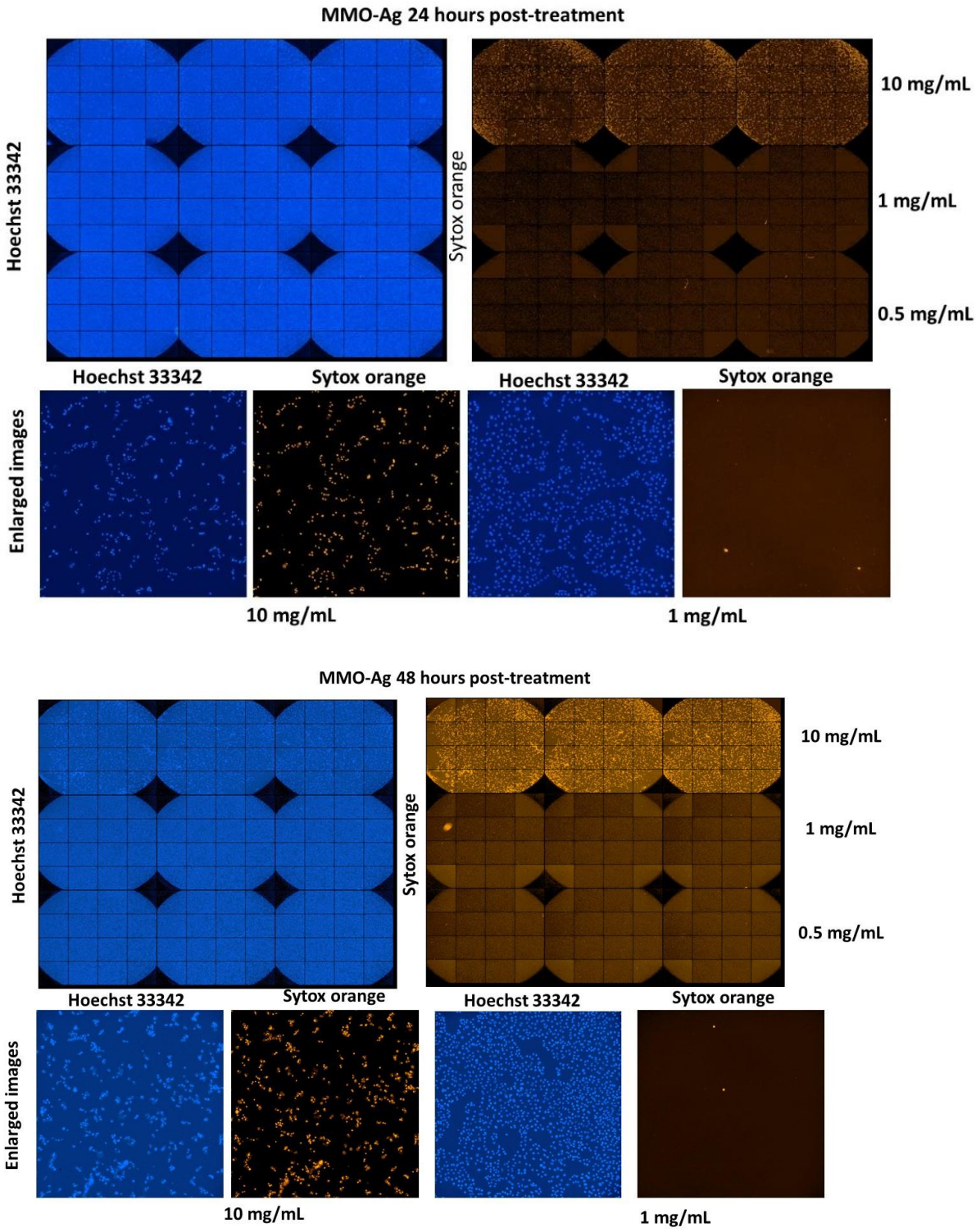

Figure S18. (a) MMO-Ag 24 hours post-treatment (b) MMO-Ag-48 hours post-treatment

Table S4. Reusability: The antibacterial activity of meltblown fabric coated with nanoformulation after various external treatments against *S. aureus* bacteria

Area of the zone of inhibition in millimetres^2(mm)^2 Diameter of plate - 90mm			
Microorganism	**Treatment method**	**Area of textile sample (mm^2)**	**Area of Zone of inhibition(mm^2)**
S. aureus	UV treatment for 30 min	12	60
		15	90
		16	81
	Exposure of Sunlight 3h	16	420
		12	380
		25	441
	Heating at 85°C	8	90
		16	110
		12	100

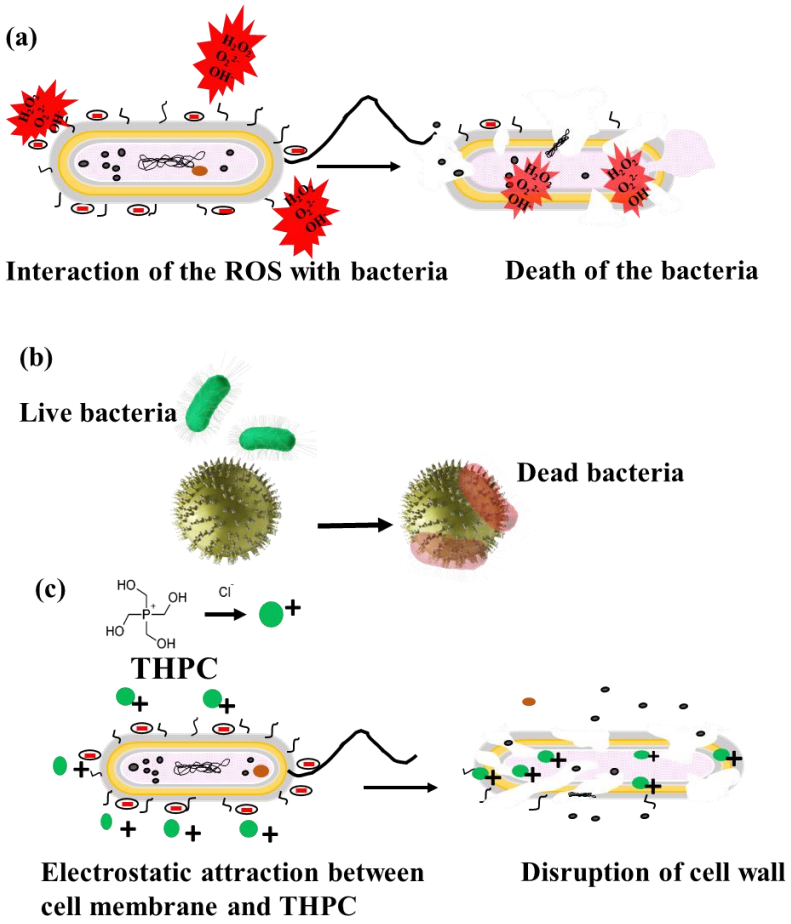

Figure S19. Schematic of the plausible mechanism of antimicrobial action of MMO-Ag. (a) Effect of ROS (b) Mechano-bactericidal effect (c) Electrostatic interaction of THPC with the bacterial cell membrane.

$$MMO\text{-}Ag + h\nu \longrightarrow e^- + h^+$$

$$e^- + O_2 \longrightarrow \bullet O_2^-$$

$$h^+ + H_2O \longrightarrow H^+ + \bullet OH$$

$$\bullet O_2^- + H^+ \longrightarrow \bullet HO_2$$

$$2\bullet HO_2 \longrightarrow H_2O_2 + O_2$$

$$H_2O_2 + e^- \longrightarrow \bullet OH + OH^-$$

$$Pathogen + (\bullet OH, \bullet O_2^-, h^+) \longrightarrow \text{degraded products } (H_2O + CO_2)$$

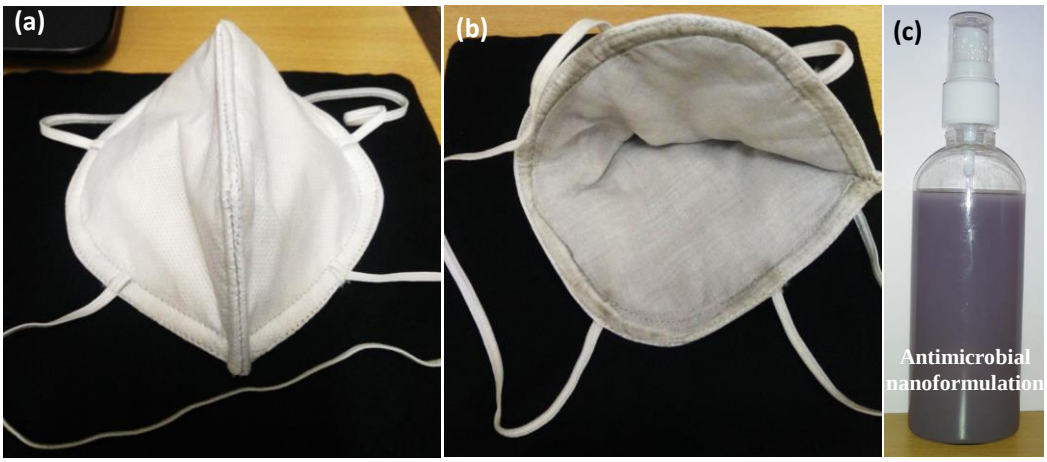

Figure S20. (a) Top view (b) Bottom view of the antimicrobial mask (c) Antimicrobial nanoformulation.

Table S5. Bacterial filtration efficiency results

Sample identification	**Average Bacterial Count**	**BFE (%)**
Mask sample coated with nanoformulation	20	99.35
Positive control (plain nonwoven fabric)	3.10×10^3	N. A

Table S6. Particle filtration efficiency of developed face mask at 0.3 micron

Particulate filtration efficiency at 0.3 microns	Nanomaterial coated mask
Percentage	99.67

Sample tested at: R.H.65%+/-2% and Temp.21°C +/- 1°C